
Förster energy transfer boosts indirect anisotropic interlayer excitons in 2L-MoSe₂/perovskite heterostructures

Yingying Chen (陈瑛瑛)¹, Zihao Jiao (焦子豪)², Haizhen Wang (王海珍)² and Dehui Li (李德慧)^{2,3*}

1 School of Science, Jimei University, Yinjiang Road 185, Xiamen 361021, China

2 School of Optical and Electronic Information, Huazhong University of Science and Technology, Luoyu Road 1037, Wuhan 430074, China

3 Wuhan National Laboratory for Optoelectronics, Huazhong University of Science and Technology, Luoyu Road 1037, Wuhan 430074, China

*Correspondence to: Email: dehuili@hust.edu.cn.

Abstract

Interlayer excitons (IXs) in two-dimensional (2D) van der Waals heterostructures have attracted considerable attention due to their unique optical and electronic properties. Owing to the spatially indirect nature, the radiative emission efficiency highly sensitive to interlayer twist angles. Further considering that their uniformly oriented out-of-plane dipole moments limit directional emission, strategies to simultaneously improve emission efficiency and induce optical anisotropy warrant in-depth investigation. In this work, we report significant photoluminescence (PL) enhancement and optical anisotropy of IXs in 2L-MoSe₂/perovskite heterostructures mediated by energy transfer from ReS₂. We attribute this enhancement to Förster resonance energy transfer (FRET), which increases the 2L-MoSe₂ emission by approximately eight-fold at room temperature, and nearly doubles the emission intensity of momentum-indirect IXs in 2L-MoSe₂/perovskite heterostructures at 78 K. Importantly, the optical anisotropy of ReS₂ can be effectively imprinted onto 2L-MoSe₂ and associated indirect IXs during the energy transfer process, yielding a linear dichroism of approximately 1.1 for both intralayer excitons and IXs with identical polarization directions. These findings expand the scope of IX study beyond direct bandgap materials with strong intrinsic emission to include systems with indirect bandgaps, offering new avenues for realizing high-performance polarization-sensitive optoelectronic devices.

Keywords: energy transfer, interlayer excitons, transition metal dichalcogenides, ReS₂, optical anisotropy

PACS: 71.35.-y

Introduction

Energy transfer and charge transfer constitute the fundamental basis of van der Waals heterostructures, giving rise to fascinating phenomena and novel physical states¹⁻³. Due to the reduced dielectric screening in layered materials, exciton states formed by charge transfer or modulated by energy transfer dominate the emission characteristics of these materials and their heterostructures⁴. These exciton states exhibit distinct luminescence properties across different systems⁵⁻⁷. For instance, monolayer transition metal dichalcogenides (TMDs) with direct bandgaps exhibit strong exciton emission with large binding energies that can sustain to room temperature⁸⁻⁹. In contrast, the emission efficiencies of few-layer TMDs possessing indirect bandgaps, as well as their heterostructures featuring indirect interlayer transitions, are generally characterized by low radiative emission efficiency¹⁰⁻¹². Therefore, improving their emission performance and efficiency are of significant research importance. In this situation, many approaches have been implemented to boost their performance, such as chemical treatment¹³, dielectric and strain engineering¹⁴⁻¹⁵, plasmonic enhancement¹⁶, cavity integration¹⁷, electrostatic doping¹⁸, and introducing strong light-matter interactions to form polaritons¹⁹, moiré excitons²⁰, or single photon emitters²¹. Among these, energy transfer, referring to donor-acceptor exchange electronic excitation, appears highly competitive owing to its lossless and low-cost nature³. This phenomenon has been extensively discussed in quantum dots system, and subsequently extends to van der Waals (vdW) heterostructures²²⁻²³. Generally, there are two types of energy transfer according to their different working mechanism, including Förster type which relies on dipole-dipole coupling over long distances (~10 nm), and Dexter type which involves electron exchange over short distances (~1 nm). These energy transfer processes have been demonstrated to efficiently improve their emission performance, which can be further modulated by external electric field²⁴, magnetic field²⁵, electrostatic gating²⁶, strain^{15, 27} or special intermediate states such as dark²⁸ or

entangled states²⁹. These findings broaden the scope of optoelectronic applications in light-emitting diodes³⁰, solar cells³¹, photodetectors³² and phototransistors³³.

In particular, interlayer excitons (IXs) in vdW heterostructures, characterized by spatially indirect natures exhibiting long lifetimes and repulsive dipolar interaction, have attract intensive attention³⁴. Recently, several studies have demonstrated the enhanced IX emission in TMD-based heterostructures³⁵⁻³⁶. Most investigations have concentrated on momentum-direct IXs or those with small twist angles in TMD heterobilayers that already possesses strong radiative emission, while momentum-indirect IXs in few-layer TMD-based heterostructures remain rarely discussed. Moreover, studies have shown that heterostructures incorporating other 2D materials, e.g. InSe or ReS₂, facilitates the transfer of optical anisotropy to IXs in addition to enhance their emission intensity by tailoring the energy transfer process³⁷⁻⁴⁰. These heterostructures exhibit strong anisotropic IX emission variations, therefore, by combining and utilizing these functional components, IXs in these systems are expected to yield novel phenomena that may attract renewed attention. Besides, considering materials with inherently weak light absorption, e.g. MoSe₂, it's of great importance to boost their emission to achieve effective optoelectronic devices.

Here, we report enhanced IX emission with induced optical anisotropy in ReS₂/hBN/2L-MoSe₂/perovskite heterostructures. By utilizing few-layer ReS₂, the exciton emission can be strongly boosted with an enhancement factor of approximately eight-fold for 2L-MoSe₂ even at room temperature. Such enhancement further extends to indirect IXs in 2L-MoSe₂/(iso-BA)₂PbI₄ heterostructure, showing a maximum enhancement factor of approximately two-fold at liquid nitrogen temperature. This enhancement capability exhibits varying power and temperature dependence between intralayer excitons in 2L-MoSe₂ and IXs in 2L-MoSe₂/(iso-BA)₂PbI₄, contingent upon the energy transfer efficiency. More importantly, the optical anisotropy of ReS₂ has been demonstrated to transfer successfully to 2L-MoSe₂ and resultant IXs with identical polarization direction and a linear dichroism of approximately 1.1. These observations facilitate the generation of momentum-indirect IXs with both strong emission and anisotropy, circumventing the strict requirement for specific rotation angles in TMD

heterobilayers to form near-direct interlayer transitions, thereby expanding their potential applications for enhancing the indirect transitions in next-generation optoelectronic devices.

Results and Discussion

Figure 1a illustrates the schematic diagram of the $\text{ReS}_2/\text{hBN}/2\text{L-MoSe}_2$ heterostructure, in which the few-layer ReS_2 and 2L- MoSe_2 are separated by a few-layer hBN flake. The heterostructure was fabricated by mechanical exfoliation from bulky crystals followed by the dry-transfer method onto a SiO_2 (300 nm)/Si substrate (Fig. 1b). According to previous literature, the band alignment between few-layer ReS_2 and 2L- MoSe_2 forms an indirect type-II configuration, favoring both energy and charge transfer processes⁴¹⁻⁴³. To eliminate the effect of charge transfer process which would quench their PL intensity, a thin layer of hBN (~10 nm) was inserted to inhibit charge transfer while permitting the occurrence of energy transfer. Figure 1c displays the PL spectra of the $\text{ReS}_2/\text{hBN}/2\text{L-MoSe}_2$ heterostructure at room temperature. While ReS_2 shows an exciton peak at 790 nm in the isolated region but becomes invisible in the heterostructure region, 2L- MoSe_2 exhibits an obvious enhancement around 810 nm in the heterostructure region. It should be noted that 2L- MoSe_2 exciton also shows a stronger emission in the hBN/2L- MoSe_2 region compared to bare 2L- MoSe_2 , mainly due to the suppression of surface disorder and defects induced between the 2L- MoSe_2 and SiO_2/Si substrate⁴⁴. Therefore, to avoid ambiguity regarding substrate influence, we focus our comparison on the PL intensity between hBN/2L- MoSe_2 and $\text{ReS}_2/\text{hBN}/2\text{L-MoSe}_2$. Notably, the indirect intralayer exciton emission shows the strongest PL intensity in the $\text{ReS}_2/\text{hBN}/2\text{L-MoSe}_2$ heterostructure. Combining the hBN insertion and the observed quenched ReS_2 emission, this enhanced emission in this heterostructure can be attributed to the non-radiative energy transfer from few-layer ReS_2 to 2L- MoSe_2 , facilitated by the significant spectral overlap between the ReS_2 absorption and 2L- MoSe_2 emission⁴⁵⁻⁴⁶. Such energy transfer should be ascribed to the Förster type according to our previous study in the $\text{ReS}_2/\text{hBN}/1\text{L-MoSe}_2$ device⁴⁷, in which the ~10 nm thickness of hBN spacer allows optimal and efficient dipole-dipole coupling⁴⁸ while effectively eliminating the possibility of Dexter type energy transfer

or charge tunneling. Notably, although 2L-MoSe₂ possesses a momentum-indirect bandgap, its direct and indirect bandgap values are almost degenerate⁴⁹. At finite temperatures, due to the layer decoupling caused by interlayer thermal expansion⁴⁵, the direct K–K transition dominates its exciton emission in the PL spectra. Consequently, the Förster resonance energy transfer (FRET) from ReS₂ preferentially populates these direct exciton states, thereby boosting the observed exciton emission intensity. Moreover, this PL enhancement differs from local interfacial charge transfer or heterostructure inhomogeneity since the uniform enhanced emission across the heterostructure region has been demonstrated in our previous work⁴⁷.

To quantify the PL enhancement, we define the PL enhancement factor as $R = I_{HS}/I_M$, where I_{HS} is the PL intensity of ReS₂/hBN/2L-MoSe₂ heterostructure and I_M represents the constituent reference hBN/2L-MoSe₂ emission intensity. Here, we compare ReS₂/hBN/2L-MoSe₂ with hBN/2L-MoSe₂ but not bare 2L-MoSe₂ to eliminate the influence of dielectric environment variation. All samples share the same hBN dielectric interface and the same hBN/SiO₂ dielectric condition underneath. Interestingly, we observe that this enhancement factor decreases with increasing excitation power. As shown in Figure 1d, 2L-MoSe₂ emission shows pronounced enhanced PL intensity under the excitation power of 82.8 μ W and moderate enhancement with the power of 8020 μ W. We further perform the power-dependent PL studies to elucidate the in-depth energy transfer mechanism. While emission intensities of both hBN/2L-MoSe₂ and ReS₂/hBN/2L-MoSe₂ increasing with increasing incident power, the rate of increase for ReS₂/hBN/2L-MoSe₂ is notably smaller (Figure 1e). Further fitting PL intensity with incident power using the power law $I = P^\alpha$, where I , P and α donates the PL intensity, laser power and power index, respectively. We determined that the α value of 2L-MoSe₂ emission in ReS₂/hBN/2L-MoSe₂ and hBN/2L-MoSe₂ regions are 0.6 and 0.9, respectively. The detailed power-dependent PL comparisons are provided in Fig. S1. Although lasing heating effects may account for some reason for this behavior at high power range above 1 mW, the energy transfer plays an important role at elevated powers. Figure 1f summarizes the enhancement

factor trend across this excitation power range, which shows a maximum $R \approx 8.2$ at $82.8 \mu\text{W}$ and minimum $R \approx 2.2$ at $8020 \mu\text{W}$. This decreased enhancement may arise from the intense energy transfer that inducing large exciton density, leading to exciton-exciton annihilation at sufficiently high excitation powers thus reducing α value. These observations further validate the contribution of FRET to this PL enhancement and rule out the effect of dielectric environment variations as it should be power-independent. We also note that such enhancement factor is smaller than that in our previously reported $\text{ReS}_2/\text{hBN}/1\text{L-MoSe}_2$ heterostructure which exhibits a ~ 58.7 -fold enhancement⁴⁷. The smaller spectral overlap between the absorption of 2L-MoSe_2 and the emission of ReS_2 , as well as the indirect nature of 2L-MoSe_2 , likely contribute to this moderate energy transfer efficiency and PL enhancement. Nevertheless, FRET remains an effective and non-destructive method for addressing weak emission especially in indirect system, which can improve radiative emission efficiency and yield a large relative enhancement factor.

Interestingly, further stacking a thin flake of 2D perovskite layer can induce intriguing phenomena (Fig. 2a). As we observed in our previous work, TMD/perovskite heterostructures can form robust IXs irrespective of stacking angles and lattice mismatch⁵⁰⁻⁵¹. In this case, the IX emission in the TMD/perovskite heterostructure is expected to be efficiently boosted through the energy transfer from ReS_2 . To validate this assumption, we fabricated a $\text{ReS}_2/\text{hBN}/2\text{L-MoSe}_2/(\text{iso-BA})_2\text{PbI}_4$ heterostructure using the same assembly methods (iso-BA represents iso-butylamine with a chemical formula of $\text{C}_4\text{H}_9\text{NH}_3$) (Fig. 2b). As shown in Fig. 2c, 2L-MoSe_2 and $(\text{iso-BA})_2\text{PbI}_4$ can form type-II heterostructures with a momentum-indirect nature, enabling the formation of indirect IXs, consistent with our previous work^{11, 50}. Since the inserted hBN layer allows energy transfer from ReS_2 to $2\text{L-MoSe}_2/(\text{iso-BA})_2\text{PbI}_4$ heterostructure (hereafter referred as HS) and blocks charge transfer from ReS_2 to HS, such energy transfer is anticipated to manipulate the optical performance of IX emission.

We subsequently carried out PL measurements at 78 K, as shown in Fig. 2d, while hBN/HS shows a peak around 775 nm corresponding to the intralayer exciton of 2L-MoSe_2 , $\text{ReS}_2/\text{hBN}/\text{HS}$ exhibit an additional peak near 795 nm and a strong peak around

777 nm that can be ascribed to the superposition of emission from few-layer ReS₂ and 2L-MoSe₂^{45, 52}. Similar phenomena can be observed in the ReS₂/hBN/2L-MoSe₂ heterostructure, which shows enhanced overall emission intensity due to the efficient energy transfer (Fig. S2). Importantly, at the low energy side, a pronounced broad peak appears with a central peak at 925 nm, which can be ascribed to IXs in hBN/HS according to their band alignment^{41, 43}. Notably, this IX emission exhibit almost two-fold PL enhancement in the presence of ReS₂-integrated heterostructure. We attribute this enhanced emission to energy transfer from ReS₂ to the heterostructure, enabling momentum-indirect IXs in ReS₂/hBN/HS with increased emission intensity. Specifically, considering the in-plane exciton nature of ReS₂ and out-of-plane nature of IXs, the energy and charge transfer process can be described as follows: (1) initial exciton generation in 2L-MoSe₂ via FERT from ReS₂ to 2L-MoSe₂ to form intralayer hot excitons, predominantly populating the direct states with a fraction evolving into the indirect states; (2) rapid intralayer thermalization and intervalley scattering in 2L-MoSe₂; (3) charge transfer occurs at the type-II 2L-MoSe₂/(iso-BA)₂PbI₂ interface to form momentum-indirect IXs. Since the hBN layer hinders the direct charge transfer from ReS₂ to HS, FRET provides more energy to 2L-MoSe₂ to increase the exciton population, thus enhancing the subsequent IX emission.

To support this hypothesis, we performed power-dependent PL studies under 633 nm laser excitation at 78 K. As shown in Fig. 2e, the power dependence of IXs in ReS₂/hBN/HS and hBN/HS exhibit divergent tendencies with a turning point around the power of 200 μ W. While IXs in hBN/HS show a uniform slope around 0.5, IXs in ReS₂/hBN/HS exhibit a larger slope of \sim 0.6 below the power of 200 μ W and a smaller slope of \sim 0.4 above the power of 200 μ W. Furthermore, the peak wavelength of IXs also shows a large shift range of 43 nm in ReS₂/hBN/HS, significantly larger than the 18 nm shift range observed for IXs in hBN/HS (Fig. S3). We further calculated the enhancement factor by comparing the PL intensity between ReS₂/hBN/HS and hBN/HS in Figure 2f. As expected, the enhancement factor initially rises with increasing incident power, reaching a maximum enhancement factor of \sim 1.8 under the power of 200 μ W, followed by a decrease at elevated powers. This power dependence contrasts

significantly with 2L-MoSe₂ exciton emission shown in Fig. 1f, but exactly explains the different slope values in Fig. 1e. Since ReS₂/hBN/2L-MoSe₂ shows largely enhanced emission intensity under low power conditions, the IX density in ReS₂/hBN/HS increase more rapidly with a large slope value. Conversely, the saturation of PL enhancement in ReS₂/hBN/2L-MoSe₂ at high power regimes results in a reduced slope value for IXs in ReS₂/hBN/HS. We should note that this enhancement factor is smaller than that of ReS₂/hBN/2L-MoSe₂, but still comparable to IXs in the previously reported ReS₂/hBN/1L-MoSe₂/(iso-BA)₂PbI₄ device⁴⁷ and other ReS₂/MoS₂ heterostructure⁴⁰. Besides, this observation cannot be simply attributed to the heterostructure inhomogeneity as the interface defect states should not exhibit this unique power-dependent trend.

To further explore the energy transfer efficiency and its influence on PL enhancement, we carried out the temperature-dependent PL studies of both ReS₂/hBN/2L-MoSe₂ and ReS₂/hBN/HS. As show in Fig. S4, the exciton peak in ReS₂/hBN/2L-MoSe₂ gradually redshifts with increasing temperature, consistent with bandgap narrowing in conventional semiconductors. Interestingly, due to relatively close exciton emission in few-layer ReS₂ and 2L-MoSe₂, these two exciton peaks become distinguishable only at low temperature (Fig. S2). As temperature increases, due to the energy transfer from ReS₂ to 2L-MoSe₂ depending on the original PL intensity of ReS₂ and the absorption-emission spectral overlap between ReS₂ and 2L-MoSe₂, the exciton emission exhibit contrasting enhancement behavior. Specifically, the PL intensities of both hBN/2L-MoSe₂ and ReS₂/hBN/2L-MoSe₂ initially decreases with increasing temperature, reaching a minimum at 200 K, before increasing up to room temperature (Fig. 3a), coinciding with the sudden reduction in spectral overlap ratio around 200 K, similar to that in ReS₂/hBN/1L-MoSe₂ reported before. This observation also suggests that although enhanced phonon-assisted indirect transitions increase non-radiative recombination with increasing temperature in 2L-MoSe₂, efficient energy transfer increase the radiative recombination rate, enabling increased PL intensity of 2L-MoSe₂ at elevated temperatures.

By comparing the PL intensity of ReS₂/hBN/2L-MoSe₂ with that of hBN/2L-MoSe₂, we can obtain the PL enhancement factor as a function of temperature, as shown in Fig. 3b. This enhancement factor gradually increases with increasing temperature, but shows a sudden drop at 200 K, followed by a continuous increase to a maximum value at room temperature. These observations indicate that the PL enhancement in the ReS₂/hBN/2L-MoSe₂ heterostructure indeed originates from energy transfer from ReS₂ to 2L-MoSe₂, which is related to the energy transfer efficiency relying on the spectral overlap between ReS₂ and 2L-MoSe₂ and total energy of the donor and acceptor system. We should note that this PL enhancement in ReS₂/hBN/2L-MoSe₂ at low temperature is comparatively moderate relative to their monolayer MoSe₂-based counterparts. This phenomenon may be attributed to three reasons: 1) the small bandgap of 2L-MoSe₂ reduces the overlap between its absorption spectrum and the emission spectrum of ReS₂, resulting a lower the energy transfer efficiency; 2) the indirect bandgap nature at low temperatures limits the intrinsic emission efficiency of 2L-MoSe₂ itself, which further impacts the energy transfer efficiency in the ReS₂/hBN/2L-MoSe₂ heterostructure; 3) both 2L-MoSe₂ and few-layer ReS₂ require phonon-assisted transition upon excitation, thereby complicating the energy transfer process. Nevertheless, despite these limitations, this energy transfer mechanism effectively improves the emission efficiency of the indirect semiconductors.

In contrast, IXs in ReS₂/hBN/HS exhibit completely opposite temperature dependence. As shown in Fig 3c, the IX emission intensity decreases monotonically with increasing temperature for both ReS₂/hBN/HS and hBN/HS. This observation can be ascribed to the gradually weakened interlayer coupling, leading to reduced electron-hole wave function overlap, thereby decreasing radiative recombination rate and resulting in low emission intensity at elevated temperatures, which becomes distinguishable above 220 K. We also calculated the enhancement factor as function of temperature. As shown in Fig. 3d, this enhancement factor maintains a relatively constant value at approximately 1.1 across varying temperature. We should note that these R values were acquired under the laser power of 2 mW to ensure visible IX emission due to the significant reduction in indirect IX emission at elevated

temperatures. As indicated in Fig. 2f, the enhancement factor decreases as the incident power exceeds 200 μW ; therefore, a smaller enhancement factor is observed in Fig. 3d. Nevertheless, this result does not affect our observation of the enhancement factor on temperature dependence. It is worth noting that this constant PL enhancement contrasts significantly with the increasing trend observed in $\text{ReS}_2/\text{hBN}/2\text{L-MoSe}_2$, which can be attributed to the interplay between varying energy transfer efficiency and band alignment with increasing temperature. As show in Fig. S5, the IX emission initially blueshifts as temperature increases to 140 K, and then redshifts. This behavior contradicts the expectations of a simple reduction in interlayer bandgap as previously reported⁵⁰, which should be explained by the shifting conduction band minimum of 2L-MoSe₂ from Γ -K to K point with increasing temperature⁴³. Below 140 K, the shift drives the blueshift; above 140 K, as the conduction band minimum of 2L-MoSe₂ settles at the K point, the IX peak energy follows the standard bandgap reduction and thereby redshifts with further increasing temperature. The combined effect of these complex factors renders the energy transfer efficiency in $\text{ReS}_2/\text{hBN}/\text{HS}$ relatively insensitive to temperature variations.

Furthermore, considering the anisotropic nature of ReS_2 which shows significant differences in light absorption and carrier concentration along different directions, we speculated that the optical anisotropy should be transmitted to IXs accompanied by energy transfer in $\text{ReS}_2/\text{hBN}/\text{HS}$. To validate this, we performed the polarization-resolved PL measurement by rotating a $\lambda/2$ waveplate in the excitation path to vary the polarization direction of the excitation light. The emission intensity was then collected and plotted as an anisotropic PL polar plot, as shown in Fig.4. Figure 4a displays a significant anisotropy of ReS_2 , showing a linear dichroism (defined as I_{max}/I_{min} , where I_{max} and I_{min} represent the dichroic fitted maximum and minimum intensity, respectively) of approximately 2.1. In contrast, due to the intrinsic in-plane isotropic nature of 2L-MoSe₂, hBN/2L-MoSe₂ shows uniform emission intensity that is independent of incident polarization (Fig.4b). Remarkably, both $\text{ReS}_2/\text{hBN}/2\text{L-MoSe}_2$ and $\text{ReS}_2/\text{hBN}/\text{HS}$ exhibit significant optical anisotropy with an identical linear dichroism of about 1.1. This demonstrates the successful anisotropy transfer to both

intralayer excitons and IXs, as the intrinsic IXs should be isotropic given the isotropic nature of 2L-MoSe₂ and (iso-BA)₂PbI₄. In this situation, we believe that the anisotropy transfer originates primarily from anisotropic absorption in ReS₂ to modulate this FRET process and associated exciton density. The mechanism can be described as follows: (1) anisotropic light absorption in ReS₂ which shows strongest along Re-Re chain directions to introduce an initial polarization-dependent exciton population; (2) a large amount energy transfer along the Re-Re chain direction from ReS₂ to 2L-MoSe₂; (3) exciton population modulation in 2L-MoSe₂ via FRET from ReS₂ despite its isotropic nature; (4) anisotropic IX emission from the preserved population imbalance, which achieves a higher IX density along the Re chains direction, thus resulting in net anisotropy transfer. The energy and charge transfer process can also be seen in Fig. S6.

It is also noteworthy that the polarization direction is identical in ReS₂/hBN/2L-MoSe₂ and ReS₂/hBN/HS, but differs from that of individual ReS₂, which can also be seen in another ReS₂/hBN/2L-MoSe₂ sample (Fig. S7). Nevertheless, ReS₂/hBN/2L-MoSe₂ and ReS₂/hBN/HS share identical polarization directions, which may result from a large carrier population along this specific direction in 2L-MoSe₂, and thereby promoting intralayer exciton dissociation upon excitation and subsequently facilitating IX formation in 2L-MoSe₂/(iso-BA)₂PbI₄. Although this linear dichroism decreases from ~2.1 in ReS₂ to ~1.1 in IXs that may be ascribed to potential depolarization through energy transfer and indirect IX formation process (such as intervalley scattering, phonon interactions, and etc)⁴⁷, this value is robust and comparable to IXs that reported in other ReS₂-based structures^{40, 53}. These observations suggest that energy transfer serves as an effective strategy to imprint optical anisotropy, paving the way to polarization-sensitive optical devices.

Conclusion

In summary, we have demonstrated the efficient energy transfer from ReS₂ to 2L-MoSe₂ and 2L-MoSe₂/(iso-BA)₂PbI₄ heterostructures, achieving anisotropic IXs with enhanced emission intensity in ReS₂/hBN/2L-MoSe₂/(iso-BA)₂PbI₄ heterostructures. We first established the presence of FRET in ReS₂/hBN/2L-MoSe₂, in which the PL intensity can be enhanced eight-fold at room temperature. This efficient energy

transfer subsequently amplifies momentum-indirect IX emission in 2L-MoSe₂/(iso-BA)₂PbI₄ heterostructures by nearly two-fold, enabling a distinct linear dichroism around 1.1. These observations indicate that optical anisotropy can be effectively transmitted through energy transfer in the heterostructure assembly of few-layer TMDs and 2D perovskites, enabling the realization of anisotropic exciton emission incorporated with substantially enhanced intensity. Our findings also evidence that FRET provide a solid platform for enhancing momentum-indirect transitions, offering a robust strategy for realizing highly efficient anisotropic sources in next-generation optoelectronics.

Methods

Sample preparations: ReS₂, MoSe₂ and hBN are bulk crystals were purchased from HQ Graphene while (iso-BA)₂PbI₄ bulk crystals were synthesized by solution methods according to our previous work. All constituent flakes were mechanically exfoliated from their bulky crystals on polydimethylsiloxane (PDMS) stamp and then stacked layer by layer on SiO₂/Si substrate by dry transfer methods.

Optical measurements: The optical images were captured on an Olympus microscope (BX53M). Samples were mounted in a liquid nitrogen bath cryostat (Cryo Industries of America Inc.) and were measured on a home-built Raman spectrometer (Horiba iHR-550) with a 600 g/mm grating. The PL spectra were acquired under the excitation of a 633-nm He-Ne laser with a 50× objective lens (NA = 0.65) under varying temperatures, which can be continuously tuned from 78 K to 300 K by a temperature controller (Lake Shore Cryotronics, Model 336). For polarization-resolved PL measurement, a set of polarizer (Thorlabs WP25M-VIS) and half-wave plate (Thorlabs AHWP05M-600) were used to control the polarization direction of incident laser, and a polarizer (Thorlabs WP25M-VIS) was placed in the collection optical path to eliminate the polarization of response grating and CCD.

Supporting Information

Supporting Information is available online or from the author.

Acknowledgments

The authors acknowledge the support from the National Key Research and Development Program of China (2024YFA1208500), the Hubei Provincial Natural Science Foundation (2025AFA039) and Open Project Program of Hubei Optical Fundamental Research Center (HBO2026C015), the Natural Science Foundation of Fujian province (2025J08202) and Xiamen City (3502Z202471047).

ORCID iDs

Yingying Chen <https://orcid.org/0000-0003-4519-5836>

Dehui Li <https://orcid.org/0000-0002-5945-220X>

Conflict of Interest

The authors declare no conflict of interests.

References:

- [1] Aftab S, Iqbal M Z, Hegazy H H, Azam S and Kabir F, 2023 *Nanoscale* 2023 **15** 3610–3629
- [2] Gillespie S C, van der Laan M, Poonia D, Maiti S, Kinge S, Siebbeles L D A and Schall P, 2024 *2D Mater.* 2024 **11** 022005
- [3] Bradac C, Xu Z Q and Aharonovich I, 2021 *Nano. Lett.* 2021 **21** 1193–1204
- [4] Chernikov A, Berkelbach T C, Hill H M, Rigosi A, Li Y, Aslan O B, Reichman D R, Hybertsen M S and Heinz T F, 2014 *Phys. Rev. Lett.* 2014 **113** 076802
- [5] Du W, Gong Y, Wang A, Zhang Y, Zhang Z, Jiang C, Bao X, Zeng X, Wu B, Zhao G, Fu J, Zheng Q, Zhang Q and Liu X, 2026 *ACS Nano* 2026 **20** 1732–1741
- [6] Zheng Y, Wang C, Tian Y, Wang X, Jiang C, Zhang Y, Gong Y, Zhong Y, Wang S, Yue S and Liu X, 2025 *Nano. Lett.* 2025 **25** 12938–12946
- [7] Gao Y, Li Y, Liu W, Yan C, Wang Q, Xin W, Xu H and Liu Y, 2025 *Chinese Physics B* 2025 **34** 097102
- [8] Nguyen-Truong H T, 2022 *Phys. Rev. B* 2022 **105** L201407
- [9] Hansen K R, Colton J S and Whittaker - Brooks L, 2023 *Adv. Opt. Mater.* 2023 **12** 2301659
- [10] Bussolotti F, Kawai H, Ooi Z E, Chellappan V, Thian D, Pang A L C and Goh K E J, 2018 *Nano Futures* 2018 **2** 032001
- [11] Yao W, Yang D, Chen Y, Hu J, Li J and Li D, 2022 *Nano. Lett.* 2022 **22** 7230–7237
- [12] Tan Q, Rasmita A, Li S, Liu S, Huang Z, Xiong Q, Yang S A, Novoselov K S and Gao W-b, 2021 *Sci. Adv.* 2021 **7** eabh0863
- [13] Bretscher H, Li Z, Xiao J, Qiu D Y, Refaely-Abramson S, Alexander-Webber J A, Tanoh A, Fan Y, Delpont G, Williams C A, Stranks S D, Hofmann S, Neaton J B, Louie S G and Rao A, 2021 *ACS Nano* 2021 **15** 8780–8789
- [14] Rhodes D, Chae S H, Ribeiro-Palau R and Hone J, 2019 *Nat. Mater.* 2019 **18** 541–549
- [15] Chen J, Xie X, Li S, Liu Z, Wang J T, He J and Liu Y, 2025 *Small* 2025 **21** 2502479

-
- [16]Pincelli T, Vasileiadis T, Dong S, Beaulieu S, Dendzik M, Zahn D, Lee S E, Seiler H, Qi Y, Xian R P, Maklar J, Coy E, Mueller N S, Okamura Y, Reich S, Wolf M, Rettig L and Ernstorfer R, 2023 *Adv. Mater.* 2023 **35** 2209100
- [17]Qian C, Troue M, Figueiredo J, Soubelet P, Villafane V, Beierlein J, Klemmt S, Stier A V, Hoefling S, Holleitner A W and Finley J J, 2024 *Sci. Adv.* 2024 **10** eadk6359
- [18]Lien D-H, Uddin S Z, Yeh M, Amani M, Kim H, Ager J W, Yablonovitch E and Javey A, 2019 *Science* 2019 **364** 468–471
- [19]Hu Z, Krisnanda T, Fieramosca A, Zhao J, Sun Q, Chen Y, Liu H, Luo Y, Su R, Wang J, Watanabe K, Taniguchi T, Eda G, Wang X R, Ghosh S, Dini K, Sanvitto D, Liew T C H and Xiong Q, 2024 *Nat. Commun.* 2024 **15** 1747
- [20]Mak K F and Shan J, 2022 *Nat. Nanotechnol.* 2022 **17** 686–695
- [21]Chuang H-J, Stevens C E, Rosenberger M R, Lee S-J, McCreary K M, Hendrickson J R and Jonker B T, 2024 *Nano. Lett.* 2024 **24** 5529–5535
- [22]Prins F, Goodman A J and Tisdale W A, 2014 *Nano. Lett.* 2014 **14** 6087–6091
- [23]Wu L, Chen Y, Zhou H and Zhu H, 2019 *ACS Nano* 2019 **13** 2341–2348
- [24]Zou Y, Zhang Z, Wang C, Cheng Y, Wang C, Sun K, Zhang W, Suo P, Lin X, Ma H, Leng Y, Liu W, Du J and Ma G, 2024 *ACS Appl. Mater. Interfaces* 2024 **16** 30589–30597
- [25]Roberto de Toledo J, Serati de Brito C, Rosa B L T, Cadore A R, Rabahi C R, Faria Junior P E, Ferreira de Brito A C, Ghiasi T S, Ingla-Aynés J, Schüller C, van der Zant H S J, Reitzenstein S, Barcelos I D, Dirnberger F and Gobato Y G, 2025 *Nano. Lett.* 2025 **25** 13212–13220
- [26]Sun Z Y, Li Y, Xu B, Chen H, Wang P, Zhao S X, Yang L, Gao B, Dou X M, Sun B Q, Zhen L and Xu C Y, 2021 *Adv. Opt. Mater.* 2021 **9** 2100438
- [27]Kim J S, Maity N, Kim M, Fu S, Juneja R, Singh A, Akinwande D and Lin J F, 2022 *ACS Appl. Mater. Interfaces* 2022 **14** 46841–46849
- [28]Luo Z, Yi X, Jiang Y, Luo N, Liu B, Zhong Y, Tan Q, Jiang Q, Liu X, Chen S, Lu Y and Pan A, 2024 *ACS Nano* 2024 **18** 31215–31224
- [29]Zhao L Y, Xiao J M, Yang J Y, Song Z X, Zhang Y P, Wang Y, Wang H, Wang W X and Wang H Y, 2025 *Laser Photonics Rev.* 2025 **19** 2400928
- [30]Huang Y, Wang Q, Mu M, Pan L, Song P, Drafi A A, Yang W and Li Y, 2025 *Adv. Opt. Mater.* 2025 **13** 2403055
- [31]Zhang J, Zhou Q, Xie J, Zhao J, Yu J, Zhang K, Jia T, Huang F and Cao Y, 2024 *Adv. Funct. Mater.* 2024 **34** 2313722
- [32]Koyaz Y, Papadopoulos S, Moilanen A J, Ziegler J D, Taniguchi T, Watanabe K, Wang L and Novotný L, 2025 *ACS Photonics* 2025 **12** 5390–5398
- [33]Chen X, Zhao H, Fei R, Huang C, Qiao J, Sun C, Zhu H, Zhan L, Hu Z, Li S, Yang L, Tang Z, Wang L, Shi Y, Ji W, Xu J B, Gao L, Gan X and Wang X, 2025 *Sci. Adv.* 2025 **11** eadw3969
- [34]Jiang Y, Chen S, Zheng W, Zheng B and Pan A, 2021 *Light: Sci. Appl.* 2021 **10** 72
- [35]Zhu J, Shen F, Chen Z, Liu F, Jin S, Lei D and Xu J, 2024 *ACS Nano* 2024 **18** 13599–13606
- [36]Zheng T, Zhao X, Yang F, Song J, Zhao W, Zhao H and Ni Z, 2024 *ACS Photonics* 2024 **11** 580–585

-
- [37] Zhang C, Wu K, Wu L, Cao G, Liu X, Zhang C, Wu S, Yuan X, Zhang L, Li X and Yang J, 2025 *Small* 2025 **21** 2411761
- [38] Zhang X, Xie X, Li S, Chen J, He J, Liu Z, Wang J T and Liu Y, 2025 *Nano Res.* 2025 **18** 2400928
- [39] Xie X, Ding J, Wu B, Zheng H, Li S, He J, Liu Z, Wang J T and Liu Y, 2023 *Appl. Phys. Lett.* 2023 **123** 222101
- [40] Luo Y, Su W, Chen F, Wu K, Zeng Y and Lu H-W, 2023 *ACS Appl. Mater. Interfaces* 2023 **15** 54808–54817
- [41] Jones L A H, Xing Z, Swallow J E N, Shiel H, Featherstone T J, Smiles M J, Fleck N, Thakur P K, Lee T-L, Hardwick L J, Scanlon D O, Regoutz A, Veal T D and Dhanak V R, 2022 *J. Phys. Chem. C* 2022 **126** 21022–21033
- [42] Koda D S, Bechstedt F, Marques M and Teles L K, 2018 *Phys. Rev. B* 2018 **97** 165402
- [43] Keyshar K, Berg M, Zhang X, Vajtai R, Gupta G, Chan C K, Beechem T E, Ajayan P M, Mohite A D and Ohta T, 2017 *ACS Nano* 2017 **11** 8223–8230
- [44] Raja A, Waldecker L, Zipfel J, Cho Y, Brem S, Ziegler J D, Kulig M, Taniguchi T, Watanabe K, Malic E, Heinz T F, Berkelbach T C and Chernikov A, 2019 *Nat. Nanotechnol.* 2019 **14** 832–837
- [45] Tongay S, Zhou J, Ataca C, Lo K, Matthews T S, Li J, Grossman J C and Wu J, 2012 *Nano. Lett.* 2012 **12** 5576–5580
- [46] Schiettecatte P, Poonia D, Tanghe I, Maiti S, Failla M, Kinge S, Hens Z, Siebbeles L D A and Geiregat P, 2021 *J. Phys. Chem. C* 2021 **125** 20993–21002
- [47] Wang H, Jiao Z, Jin C, Jiang K and Li D, 2026 *Small* 2026 **n/a** e10501
- [48] Karmakar A, Al-Mahboob A, Petoukhoff C E, Kravchyna O, Chan N S, Taniguchi T, Watanabe K and Dani K M, 2022 *ACS Nano* 2022 **16** 3861–3869
- [49] Yun W S, Han S W, Hong S C, Kim I G and Lee J D, 2012 *Phys. Rev. B* 2012 **85** 033305
- [50] Chen Y, Liu Z, Li J, Cheng X, Ma J, Wang H and Li D, 2020 *ACS Nano* 2020 **14** 10258–10264
- [51] Yang D, Hu J, Chen Y and Li D, 2023 *Adv. Opt. Mater.* 2023 **11** 2300398
- [52] Tongay S, Sahin H, Ko C, Luce A, Fan W, Liu K, Zhou J, Huang Y S, Ho C H, Yan J, Ogletree D F, Aloni S, Ji J, Li S, Li J, Peeters F M and Wu J, 2014 *Nat. Commun.* 2014 **5** 3252
- [53] Che Z, Deng W, Li J, Zhao C, Wang F, Wu Y, Wang Q J, Qiu C and Zhang Y, 2025 *Adv. Funct. Mater.* 2025 **35** 2416994

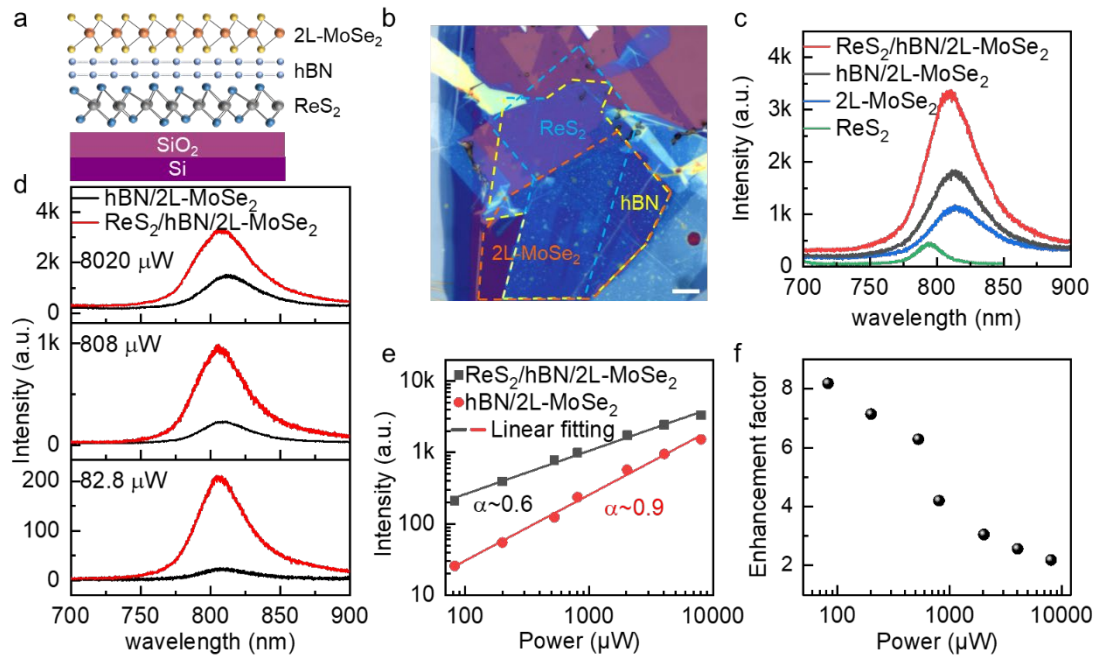


Figure 1. Energy transfer from ReS₂ to 2L-MoSe₂ to boost emission. Schematic illustration (a) and optical image (b) of the ReS₂/hBN/2L-MoSe₂ heterostructure on the SiO₂/Si substrate. The dashed orange, yellow and blue lines outline the edge of 2L-MoSe₂, few-layer hBN and multi-layer ReS₂, respectively from top to bottom. Scale bar, 10 μm. (c) PL spectra of the ReS₂/hBN/2L-MoSe₂ heterostructure and constituent components at room temperature under the excitation of 633 nm laser with a power of 800 μW. (d) PL comparison of hBN/2L-MoSe₂ and ReS₂/hBN/2L-MoSe₂ heterostructures under different excitation power of 633 nm laser. (e) Power-dependent emission intensity of hBN/2L-MoSe₂ and ReS₂/hBN/2L-MoSe₂ heterostructures and linear fittings. (f) Power dependence of enhancement factor in the ReS₂/hBN/2L-MoSe₂ heterostructure.

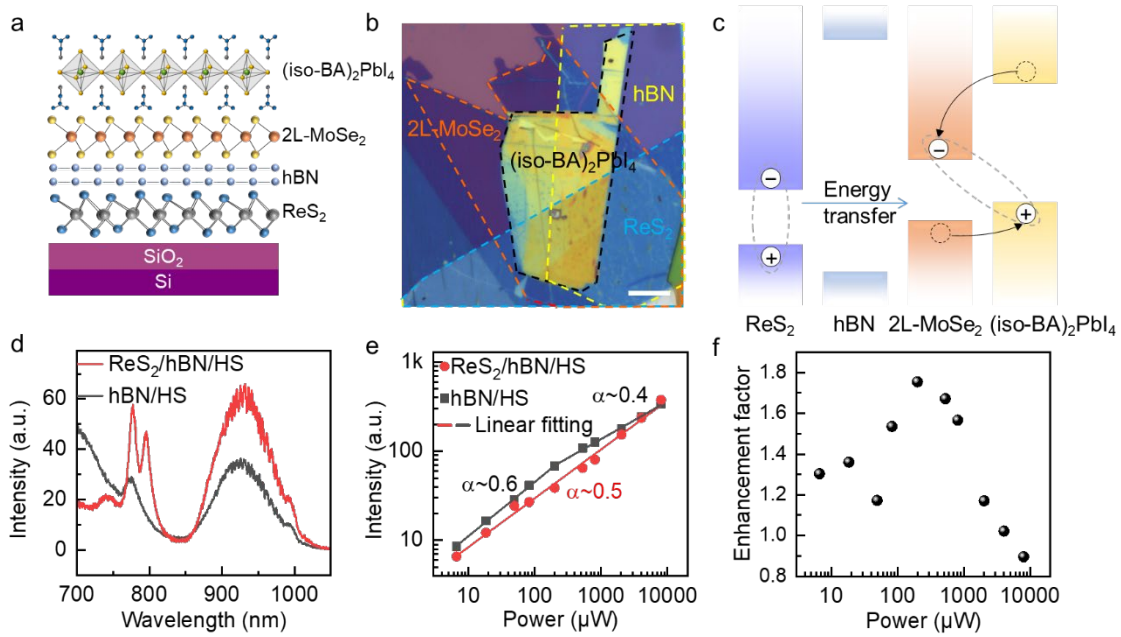


Figure 2. Enhanced IX emission in $\text{ReS}_2/\text{hBN}/2\text{L-MoSe}_2/(\text{iso-BA})_2\text{PbI}_4$ heterostructure via energy transfer. Schematic illustration (a) and optical image (b) of the $\text{ReS}_2/\text{hBN}/2\text{L-MoSe}_2/(\text{iso-BA})_2\text{PbI}_4$ heterostructure. The dashed black, orange, yellow and blue lines outline the edge of $(\text{iso-BA})_2\text{PbI}_4$ flake, 2L-MoSe_2 , few-layer hBN and multi-layer ReS_2 from top to bottom. Scale bar, $10\ \mu\text{m}$. (c) Schematic band diagram of the dynamic processes, including the charge transfer process in $2\text{L-MoSe}_2/(\text{iso-BA})_2\text{PbI}_4$ to form IXs and energy transfer from ReS_2 to $2\text{L-MoSe}_2/(\text{iso-BA})_2\text{PbI}_4$. (d) PL spectra of $\text{ReS}_2/\text{hBN}/2\text{L-MoSe}_2/(\text{iso-BA})_2\text{PbI}_4$ (abbreviated as $\text{ReS}_2/\text{hBN}/\text{HS}$) and $\text{hBN}/2\text{L-MoSe}_2/\text{HS}$ region under the excitation of $633\ \text{nm}$ with a power of $200\ \mu\text{W}$ at $78\ \text{K}$. (e) Power-dependent emission intensity of $\text{ReS}_2/\text{hBN}/\text{HS}$ and $\text{hBN}/2\text{L-MoSe}_2/\text{HS}$ and linear fittings. (f) Power dependence of enhancement factor in $\text{hBN}/2\text{L-MoSe}_2/\text{HS}$.

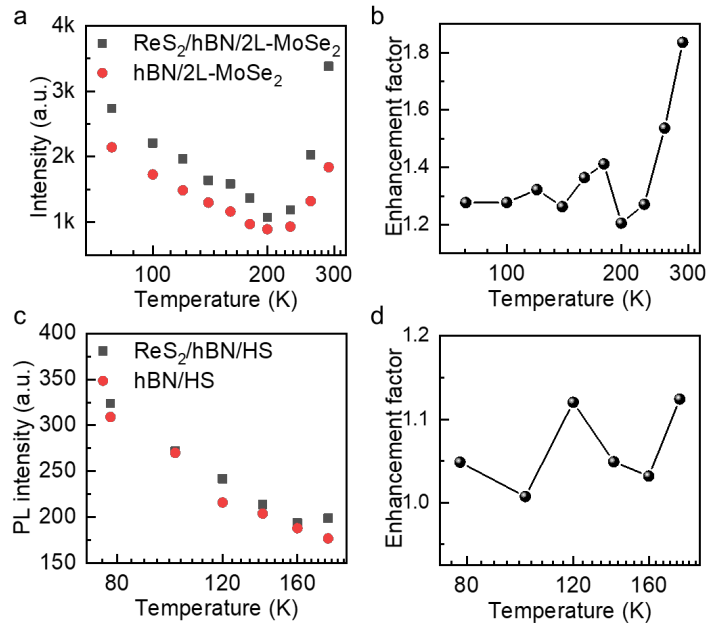


Figure 3. Temperature dependence of PL enhancement. Temperature-dependent PL intensity between different regions in ReS₂/hBN/2L-MoSe₂ (a) and ReS₂/hBN/HS (c) under the excitation of 633 nm with a power of 800 μ W. Temperature-dependent evolution of PL enhancement factor of ReS₂/hBN/2L-MoSe₂ (b) and ReS₂/hBN/HS (d) under the excitation of 633 nm with a power of 2 mW.

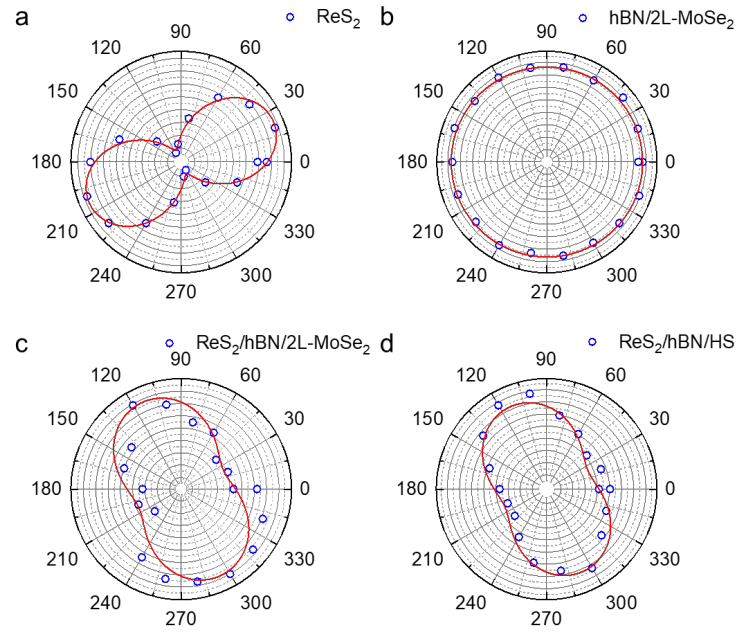


Figure 4. Transfer of optical anisotropy accompanied by energy transfer. Polar plots of polarization dependence of exciton emission intensity in ReS₂ (a), 2L-MoSe₂ (b), ReS₂/hBN/2L-MoSe₂ (c), and IXs in ReS₂/hBN/HS (d) under the excitation of 633 nm with a power of 200 μ W at 78 K.

Supporting Information for
Förster energy transfer boosts indirect anisotropic interlayer excitons in 2L-
MoSe₂/perovskite heterostructures

Yingying Chen¹, Zihao Jiao², Haizhen Wang² and Dehui Li^{2,3*}

1 School of Science, Jimei University, Yinjiang Road 185, Xiamen 361021, China

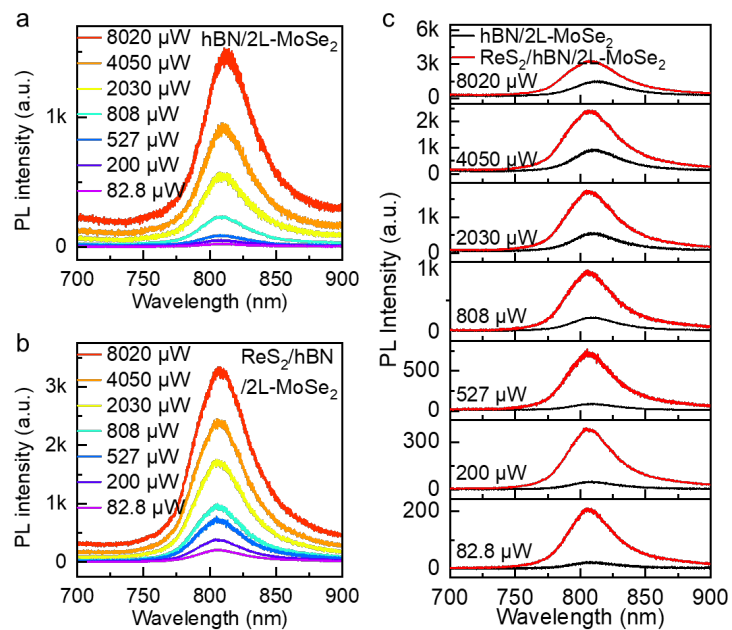
*2 School of Optical and Electronic Information, Huazhong University of Science and
Technology, Luoyu Road 1037, Wuhan 430074, China*

*3 Wuhan National Laboratory for Optoelectronics, Huazhong University of Science
and Technology, Luoyu Road 1037, Wuhan 430074, China*

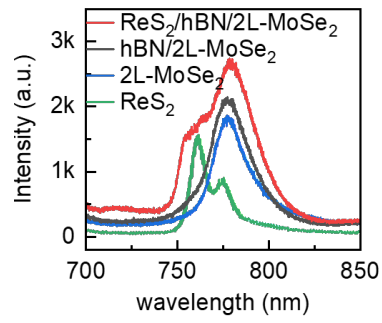
*Correspondence to: Email: dehuili@hust.edu.cn.

This PDF file includes:

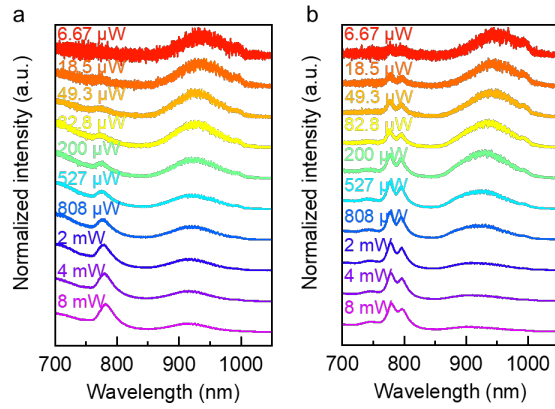
Supplementary Figs. 1 to 7



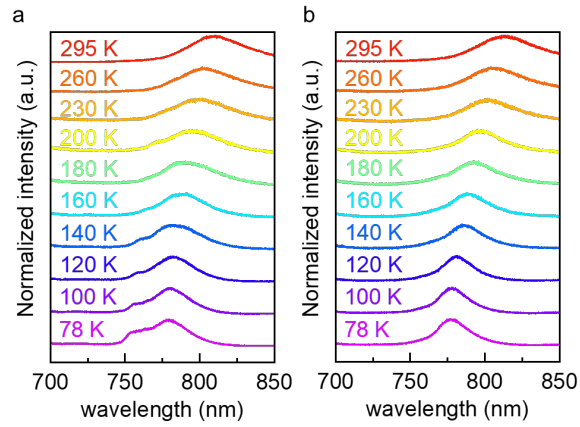
Supplementary Fig. 1 Power-dependent PL spectra of hBN/2L-MoSe₂ (a) and ReS₂/hBN/2L-MoSe₂ (b) under the excitation of 633 nm at room temperature. (c) Detailed comparison of PL spectra between hBN/2L-MoSe₂ and ReS₂/hBN/2L-MoSe₂ under varying incident power.



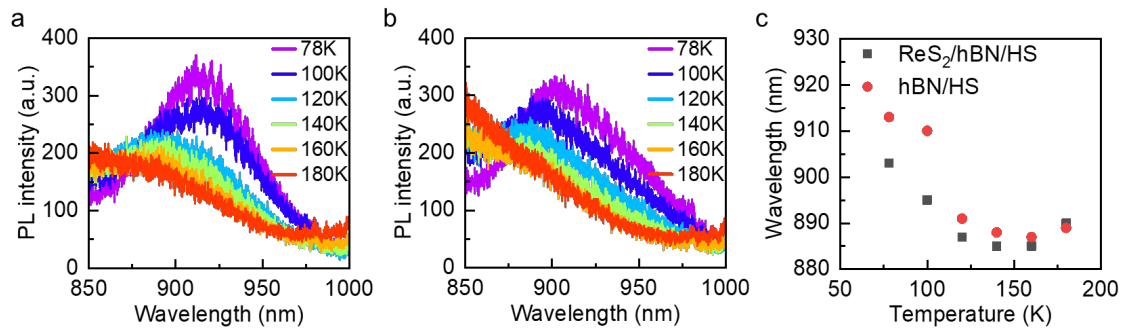
Supplementary Fig. 2 PL spectra of the ReS₂/hBN/2L-MoSe₂ heterostructure and constituent individual regions under the excitation of 633 nm with the power of 800 μ W at 78 K.



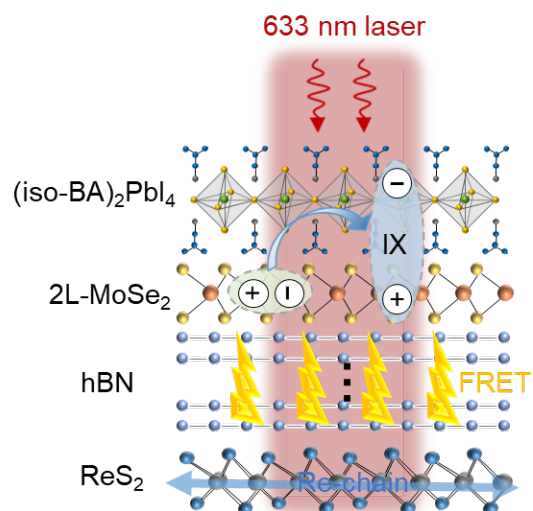
Supplementary Fig. 3 Normalized power-dependent PL spectra of hBN/2L-MoSe₂/(iso-BA)₂PbI₄ (a) and ReS₂/hBN/2L-MoSe₂/(iso-BA)₂PbI₄ (b) under the excitation of 633 nm at 78 K.



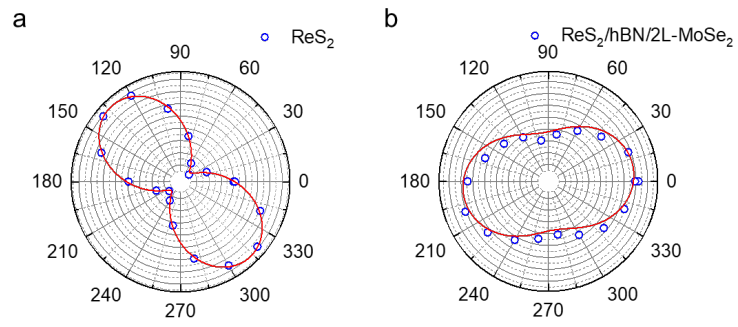
Supplementary Fig. 4 Normalized temperature-dependent PL spectra of hBN/2L-MoSe₂ (a) and ReS₂/hBN/2L-MoSe₂ (b) under the excitation of 633 nm with a power of 800 μ W.



Supplementary Fig. 5 Temperature-dependent PL spectra of hBN/2L-MoSe₂/(iso-BA)₂PbI₄ (a) and ReS₂/hBN/2L-MoSe₂/(iso-BA)₂PbI₄ (b) under the excitation of 633 nm with a power of 2 mW. (c) Central peak wavelength of hBN/2L-MoSe₂/(iso-BA)₂PbI₄ and ReS₂/hBN/2L-MoSe₂/(iso-BA)₂PbI₄ as a function of temperature.



Supplementary Fig. 6 Schematic illustration of the energy and charge transfer processes.



Supplementary Fig. 7 Polar plots of linear polarization-dependent PL intensity of another ReS₂ (a) and ReS₂/hBN/2L-MoSe₂ (b) at room temperature, which shows a linear dichroism of ~ 2.0 and ~ 1.1 , respectively.